

Fracture toughness of the tensile and compressive fibre failure modes in laminated composites

S T Pinho ^a, P Robinson ^a, L Iannucci ^a

^a*Department of Aeronautics, South Kensington Campus, Imperial College London, SW7 2AZ, London, U.K.*

Abstract

The fracture toughnesses associated with fibre tensile failure and compressive fibre kinking in a T300/913 carbon-epoxy laminated composite are measured using compact tension and ‘compact compression’ tests respectively. The specimen strain fields were monitored using a digital speckle photogrammetry system during the tests. The damage present in the specimens after the tests was investigated using C-scan and optical and scanning electron microscopy. The initiation and propagation values of the tensile fibre failure critical energy release rate were determined as 91.6 kJ/m² and 133 kJ/m² respectively. For fibre compressive kinking, an initiation value of 79.9 kJ/m² was obtained, but no meaningful propagation values could be determined. In both cases, the test results showed low scatter.

Key words: B Fracture toughness, Fibre failure

Email addresses: silvestre.pinho@imperial.ac.uk (S T Pinho),
p.robinson@imperial.ac.uk (P Robinson), l.iannucci@imperial.ac.uk (L

1 Introduction

Fibre breaking can take place during longitudinal tension or compression and, for carbon/epoxy systems, the energy consumed by these failure processes is much larger than for failures involving any matrix or matrix-fibre bond failure. In compression, fibre breaking usually occurs as a result of the kinking process. Experimental determination of the fracture toughness associated with both these fibre failure modes (tensile failure and compressive kinking) is important for material characterization and for numerical modelling. Currently, there are no standards to determine these properties.

Leach and Moore [1] used three-point bend specimens with a $(0)_{40}$ layup to measure the fracture toughness of the tensile fibre failure mode of a carbon/ PEEK composite, and reported a mode I critical energy release rate of 26 kJ/m^2 . The technique used to introduce a pre-crack in the specimen was not discussed by the authors. Jose et al. [2] used Compact Tension (CT) specimens (see Fig. 1(a)) made of M55J/ M18 carbon/epoxy with layup $(0, 90)_{15}$, to determine the fracture toughness associated with tensile failure of the $(0, 90)_{15}$ laminate. They created the pre-crack in two steps: a notch was cut with a disc cutter and a razor blade was then used to give a sharp starter, but the authors did not specify whether the blade was tapped or used in a sawing motion. The mode I critical energy release rate reported by Jose et al. for the laminate is 15.94 kJ/m^2 . This value corresponds to the mode I critical energy release rate for fibre fracture in the 0° layers combined with matrix crack propagation in the 90° layers. Assuming that those energies are additive (which is to say, neglecting the interactions between the different layers that are failing in different Iannucci).

failure modes), and that the matrix tensile toughness is similar in magnitude to the (interlaminar) mode I critical energy release rate ($\approx 0.2 \text{ kJ/m}^2$), the critical energy release rate for the fibre tensile failure mode of M55J/ M18 carbon/epoxy is about 31.7 kJ/m^2 .

Soutis et al. [3,4] carried out a kink-band propagation test using a centre-notched compression specimen. Different lengths for the notch were used but similar values of fracture toughness were observed, which was interpreted as supporting the concept of compressive fracture toughness. For a T800/924C laminate with $(0, 90_2, 0)_{3S}$ layup, the critical energy release rate for the laminate was reported [5] as 38.8 kJ/m^2 . Proceeding as before, the value measured corresponds to the mode I critical energy release rate for kink-band propagation in the 0° layers, plus the critical energy release rate for matrix cracking in the 90° layers. Assuming that those energies are additive, and making the simplification that the matrix failure in the 90° layers can be represented by a single mode II matrix crack (with critical energy release rate $\approx 1 \text{ kJ/m}^2$), the critical energy release rate for kink-band formation and for T800/924C is derived from Soutis et al. [5] as about 76 kJ/m^2 .

Ratcliffe et al. [6] and Jackson and Ratcliffe [7] described the use of Compact Compression (CC) specimens (CC specimens are similar to CT specimens, but used in compression) to measure the compressive toughness of sandwich panels with unidirectional carbon-epoxy facings and honeycomb nomex core. The kink-band length was measured using Shadow Moiré Interferometry. The critical energy release rate for kinking, derived from the tests using the area method, was reported as 36.1 kJ/m^2 [6].

In the work presented in this paper, CT and CC tests were performed with

Table 1

Mechanical properties of T300/913 unidirectional laminae.

| Modulus (GPa) | | | Major Poisson's ratio |
|----------------|------------|-------|-----------------------|
| Longitudinal | Transverse | Shear | |
| 131.7 | 8.8 | 4.6 | 0.32 |

the aim of determining (i) the fracture toughness associated with tensile fibre failure and (ii) the fracture toughness associated with kink-band failure for a carbon-epoxy system.

2 Material system used

Carbon epoxy T300/913 unidirectional prepreg was used for the tests. The material properties needed for the data reduction were obtained using standard tests and are presented in Table 1 in the principal material axes.

3 Test method and data reduction

The geometry of the compact specimens used for the tension and compression toughness tests are shown in Fig. 1(a) and (b) respectively. The notch of the CC specimen, Fig. 1(b), has been widened at the left edge to avoid contact of the notch faces during compression. (Jackson and Ratcliffe [7] found that the stress intensity factor is not affected significantly by the morphology of the opening.) The layup used is $(90,0)_{8S}$ with the 0° -direction the direction parallel to the loading, as shown in Fig. 1.

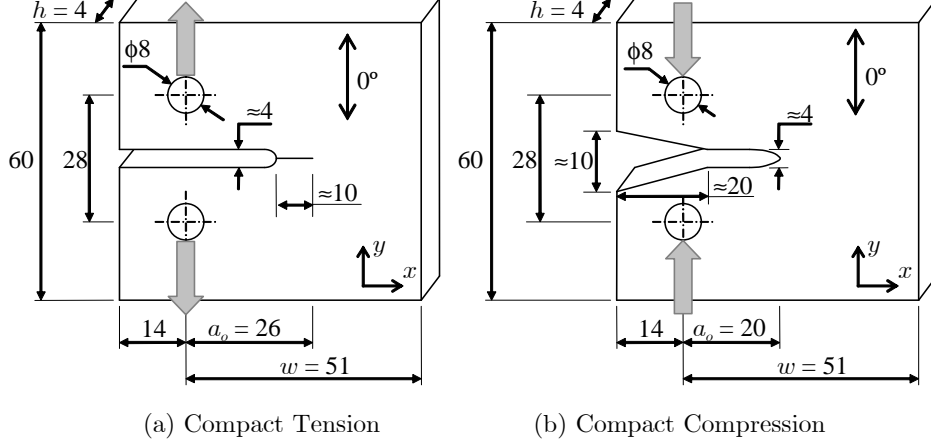


Fig. 1. Test specimen nominal dimensions (in mm) for the (a) tensile and (b) compression fibre-breaking fracture toughness tests

The data reduction for CT or CC specimens made of an orthotropic material requires particular attention. Other researchers have used the stress intensity factor approach [2,8,9], often citing the ASTM standard E399 [10] for the determination of the fracture toughness in metals using CT tests [2,8].

According to ASTM standard E399 [10], valid for an isotropic material, the critical stress intensity factor for a fracture load P , is given by

$$K_{Ic} = \frac{P}{h\sqrt{w}} f(a/w) \quad (1)$$

with

$$f(a/w) = \frac{2 + a/w}{(1 - a/w)^{1.5}} [0.886 + 4.64(a/w) - 13.32(a/w)^2 + 14.72(a/w)^3 - 5.6(a/w)^4] \quad (2)$$

where h is the thickness of the specimen, w is the dimension from the load line to the right hand edge of the specimen, as indicated in Fig. 1 and a is the crack length, whose initial value a_o is also indicated in Fig. 1. The critical

energy release rate of the laminate can be calculated from K_{Ic} as [11]

$$G_{Ic}|_{lam} = \frac{K_{Ic}^2}{\sqrt{2E_x E_y}} \sqrt{\sqrt{\frac{E_x}{E_y} + \frac{E_x}{2G_{xy}} - \nu_{xy}}} \quad (3)$$

where E_x , E_y , G_{xy} and ν_{xy} are the Young's moduli in the x and y directions (see Fig. 1), the shear modulus and the Poisson's ratio of the laminate, respectively (note that these properties are obtained from the laminae values given in Table 1 using lamination theory).

Jose et al. [2] carried out Finite Element (FE) analyses of laminate CT specimens, and compared the stress intensity factor obtained from Eq. 1 with the one obtained from FE. They concluded that the difference was small even though, when expressed in terms of energy release rate, the difference ranged from 16% to 27%, depending on the layup. The difference was attributed to the FE analysis being linear, but Eq. 1 also assumes linear elasticity and so the difference is more likely to be due to the isotropy assumption in Eq. 1.

Given the difference observed by Jose et al., an FE analysis was carried in Abaqus [12] to obtain a more accurate equation for the energy release rate. As a first step, three different models of half a CT/CC specimen were created (taking advantage of the symmetry), with different levels of mesh refinement. The three meshes have uniform square 8-noded elements (S8R5), with side $l = 1$ mm for the coarse (C) mesh, $l = 0.5$ mm for the intermediate (I) mesh and $l = 0.2$ mm for the refined (R) mesh. Mesh C is presented in Fig. 2, where it can be noted that the shape of the notch is not modelled; as mentioned before, earlier work by Jackson and Ratcliffe [7] showed that the stress intensity factor is not significantly affected by the morphology of the opening. The material properties were obtained from Table 1 using lamination theory for a $(90,0)_{8S}$ layup. All the models were assigned a unit thickness

(1 mm), and were subjected to a unit load (1 N). For a crack length $a = 26$ mm, each model was run to obtain the J-integral around the crack tip. Taking the J-integral for mesh R as a reference, the J-integral for mesh I differs in 0.014% and for mesh C in 0.026%. The application of the one-step Virtual Crack Closure Technique (VCCT) for mesh R matches the J-integral for the same mesh within less than 0.004%. Therefore, all three meshes (C, I and R) provide an accurate value of the energy release rate. The difference between the energy release rate obtained by the use of FE (J-integral, mesh R) and by the use of Eqs. 1 and 3 is 11.02%. This non-trivial difference indicates that the K_{Ic} formula of Eq. 1 which is used for isotropic materials is not always accurate for orthotropic composites.

Several models with mesh I and different values of initial crack length were run. The normalized energy release rate $f(a)$, obtained from the J-integral (J), and defined as

$$f(a) = J \cdot \left(\frac{1 \text{ mm}}{1 \text{ N}} \right)^2 \quad (4)$$

is presented in Table 2. The function $f(a)$ can be approximated by the polynomial

$$f(a) = c_3 a^3 + c_2 a^2 + c_1 a + c_0 \quad (5)$$

where the coefficients c_i are presented in Table 3 for a number of different crack length ranges together with the associated interpolation error. Finally, the critical energy release rate for each test can be obtained as

$$G_{Ic}|_{lam} = \left(\frac{P}{h} \right)^2 f(a). \quad (6)$$

For the CT tests, Eq. 6 can be used to obtain G_{Ic} as a function of crack length during propagation, provided that completely unstable propagation does not occur immediately after initiation of crack growth. For fibre kinking

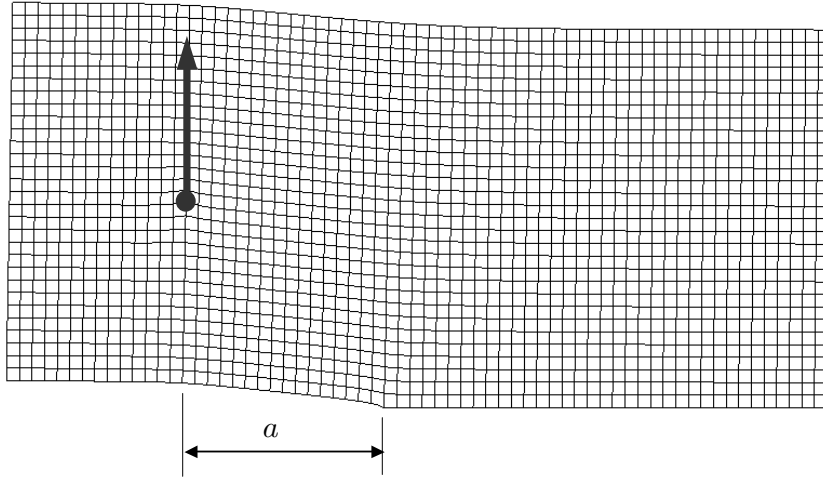


Fig. 2. Coarse FE mesh of half a CT specimen

Table 2

Normalised energy release rate $f(a)$ (m^2/kJ) for different values of crack length a (mm), obtained from FE

| | | | | | | |
|--------|-----------|-----------|-----------|-----------|-----------|-----------|
| a | 19 | 20 | 21 | 22 | 23 | 24 |
| $f(a)$ | 3.4003E-5 | 3.6753E-5 | 3.9839E-5 | 4.3320E-5 | 4.7272E-5 | 5.1788E-5 |
| a | 25 | 26 | 27 | 28 | 29 | 30 |
| $f(a)$ | 5.6984E-5 | 6.3007E-5 | 7.0043E-5 | 7.8332E-5 | 8.8187E-5 | 1.0001E-4 |
| a | 31 | 32 | 33 | 34 | 35 | 36 |
| $f(a)$ | 1.1436E-4 | 1.3196E-4 | 1.5381E-4 | 1.8132E-4 | 2.1646E-4 | 2.6207E-4 |
| a | 37 | 38 | 39 | 40 | 41 | 42 |
| $f(a)$ | 3.2238E-4 | 4.0374E-4 | 5.1609E-4 | 6.7539E-4 | 9.0839E-4 | 1.2619E-3 |
| a | 43 | 44 | | | | |
| $f(a)$ | 1.8229E-3 | 2.7642E-3 | | | | |

Table 3

Coefficients for the interpolation of $f(a)$ (m^2/kJ) for different ranges of crack length a (mm), and associated maximum error

| | c_3 | c_2 | c_1 | c_0 | error |
|------------------|-----------|--------------|-----------|------------|---------|
| $19 \leq a < 24$ | 1.1250E-8 | -5.088214E-7 | 9.7590E-6 | -4.4897E-5 | < 0.01% |
| $24 \leq a < 29$ | 4.0880E-8 | -2.6721E-6 | 6.2522E-5 | -4.7474E-4 | < 0.01% |
| $29 \leq a < 34$ | 1.7282E-7 | -1.4396E-5 | 4.1001E-4 | -3.9105E-3 | < 0.08% |
| $34 \leq a < 39$ | 1.1264E-6 | -1.1389E-4 | 3.8722E-3 | -4.4084E-2 | < 0.14% |
| $39 \leq a < 44$ | 1.6611E-5 | -1.9748E-3 | 7.8429E-2 | -1.0399E0 | < 0.80% |

however, Eq. 6 has limited meaning during propagation, because the contact stresses between the ‘faces’ of the kink band are not accounted for in the FE analysis, and neither is the damage that might propagate from the kink band. An alternative method for data reduction during propagation consists of the use of the area method in which the energy consumed during crack growth (determined from the area under the load vs. displacement curve) is divided by the area swept out by the crack front. However, the application of this method requires stable crack growth, and, in the case of the CC specimens, the calculated energy release rate will still include energy consumed by other damage modes which are also developing as the kink band advances. This results in an artificial positive trend on the R-curves as verified by Jackson and Ratcliffe [7].

Once the critical energy release rate for the laminate is obtained, the critical energy release rate corresponding to fibre tensile failure or fibre kinking is obtained by subtracting the term corresponding to matrix cracking in the 90°

layers. This procedure neglects the other damage modes such as delamination, as well as any interaction between matrix cracking and the fibre-dominated failure modes, and assumes that a single matrix crack parallel to the pre-crack occurs in the 90° layers. As before, matrix cracking in the 90° layers is assumed to occur as a single crack in mode I for the CT tests, and in mode II for the CC tests. These approximations seem reasonable, since the critical energy release rate of the fibre-dominated failure modes is much higher than that of the matrix-dominated ones. For the laminate layup used for these tests, the critical energy release rate for the fibre-dominated failure modes is thus expressed as

$$G_{Ic}|_{fibre\ tensile} = 2 G_{Ic}|_{lam\ tensile} - G_{Ic}|_{matrix\ intra} \quad (7)$$

$$G_{Ic}|_{fibre\ kinking} = 2 G_{Ic}|_{lam\ compr} - G_{IIc}|_{matrix\ intra} \quad (8)$$

where $G_{Ic}|_{lam\ tensile}$ and $G_{Ic}|_{lam\ compr}$ are the critical energy release rate for the laminate, as obtained from the tensile and compressive tests respectively, $G_{Ic}|_{matrix\ intra}$ and $G_{IIc}|_{matrix\ intra}$ are the mode I and mode II matrix-cracking intralaminar fracture toughnesses, and $G_{Ic}|_{fibre\ tensile}$ and $G_{Ic}|_{fibre\ kinking}$ are the fracture toughnesses for the fibre tensile and fibre-kinking failure modes. The mode I intralaminar critical energy release rate for through-the-thickness crack growth was found to be very similar to the interlaminar toughness between 0° plies [13], so that, for materials where the matrix-cracking intralaminar critical energy release rate is unknown, the interlaminar critical energy release rate is expected to be a good approximation of the intralaminar critical energy release rate. As noted above, in carbon/epoxy systems, the matrix failure mode toughnesses are much lower than the fibre failure toughnesses and so the last term in Eqs. 7 and 8 could be omitted without a significant loss in accuracy.

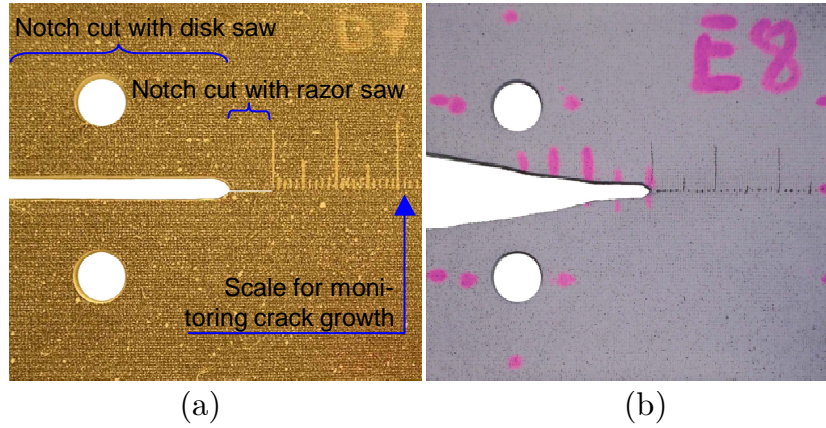


Fig. 3. Photograph of the specimens obtained for the (a) tensile and (b) compression fibre fracture toughness tests

4 Manufacture

4.1 Manufacture of the test specimens

Panels with dimensions $300 \times 150 \text{ mm}^2$ were manufactured by laying up 32 layers of prepreg (each of 0.125 mm nominal thickness), with a layup $(90, 0)_{8S}$ and cured according to the prepreg manufacturer's instructions. A wet saw was used to cut the rectangular plates to form the specimens shown in Fig. 3. The 8 mm diameter holes were produced by drilling the specimen, with it held in between two sacrificial pieces of similar composite.

For the tensile specimens, a 3-step procedure was followed to obtain the required sharp crack tip. First, a 4 mm wide notch was cut with a diamond-coated disk saw, to a total approximate length of 30 mm. Then, a 0.2 mm thick razor saw was used to obtain a thin and relatively sharp extension of the pre-crack, with a length of approximately 10 mm. Finally, a 0.1 mm thick razor blade was used to sharpen the crack tip further using a sawing action.

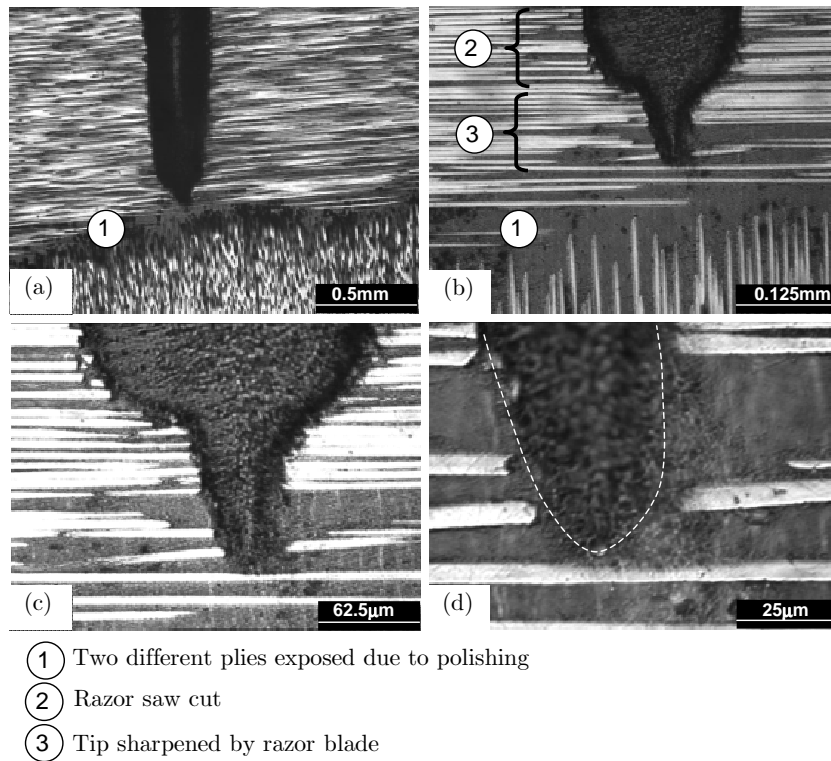


Fig. 4. Different magnifications of the pre-crack tip for the CT specimens
 Micrographs of the crack tip are presented in Fig. 4. For the compression specimens, a notch as shown in Fig. 3(b) was obtained with the disk saw.

A speckle pattern was created on one face of each specimen using white and black ink sprays. Two different types of pattern were tried: black spots on a white background and white spots on a black background. The former was obtained by painting one side of the specimen in white and then using the black-ink spray to obtain the speckle pattern. This process led to a maximum contrast which is beneficial for the photogrammetry system software monitoring each point of the specimen. However, in the tensile tests, the white ink tended to peel at the crack tip during crack propagation. For these cases, the reverse pattern was used (white spots on a black background), by simply using the white spray to create the white spots on the black surface of the composite. The contrast is in this case not as good as the previous one, but

no peeling occurs at the crack tip during propagation.

Finally, a 1 mm increment scale was drawn onto each specimen to monitor the crack length during the test, and the actual dimensions of each specimen were measured individually.

5 Experimental setup

Six CT and six CC tests were carried out in an Instron machine, with a 10 kN load cell. Two strong light sources were used to illuminate the surface of the specimen.

A CCD camera was used to view a magnified image of the area of the specimen containing the crack-growth scale on a TV. This magnified image was used together with an event-marker connected to the data logger, to monitor the crack growth.

The photogrammetry system (Aramis) was positioned to examine the surface of the specimen. This system allowed the strain field in the specimens to be recorded during the tests and was used to check for damage not readily visible in the specimens, and to help locate the tip of the crack/kink-band. The CT and CC specimens were loaded at a displacement-rate of 0.5 mm/min.

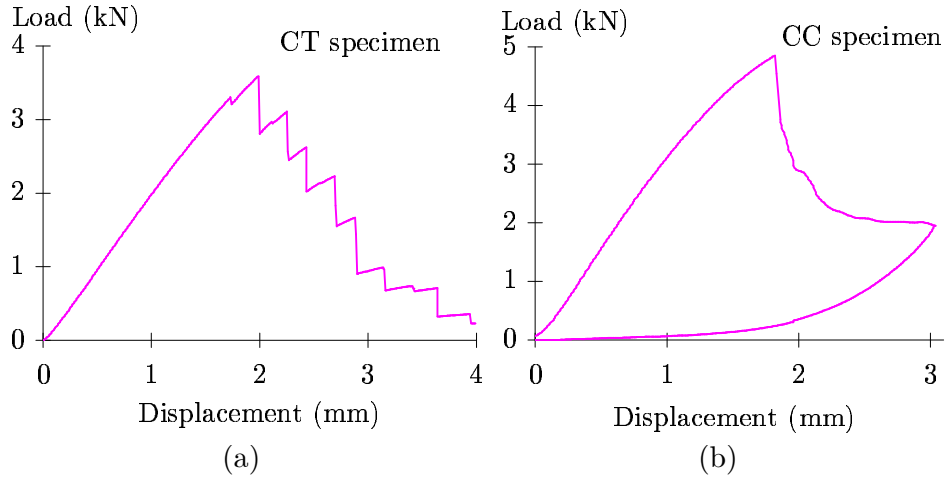


Fig. 5. Typical load vs. displacement curves for a (a) CT and (b) CC specimens

6 Results

6.1 Tensile tests

For the CT specimens tested, crack growth was not smooth nor continuous: instead, several crack jumps of a few millimeters each time were observed, Fig. 5(a). The TV monitor and event marker permitted the recording of the propagation load for each value of crack length where the crack had stopped.

The first specimen tested had a black speckle pattern on a white background. As the crack proceeded, the white ink peeled from the specimen on the vicinity of the crack, and the photogrammetry system thus failed to map the strains on the area of most interest, Fig. 6(a) and (b). For all other tensile specimens, a white speckle on the natural black surface of the composite was used. This speckle had a lower contrast, but still allowed the identification of the crack tip as no peeling occurred, Fig. 6(c) and (d).

The R-curves obtained from the tensile tests are shown in Fig. 7. The average

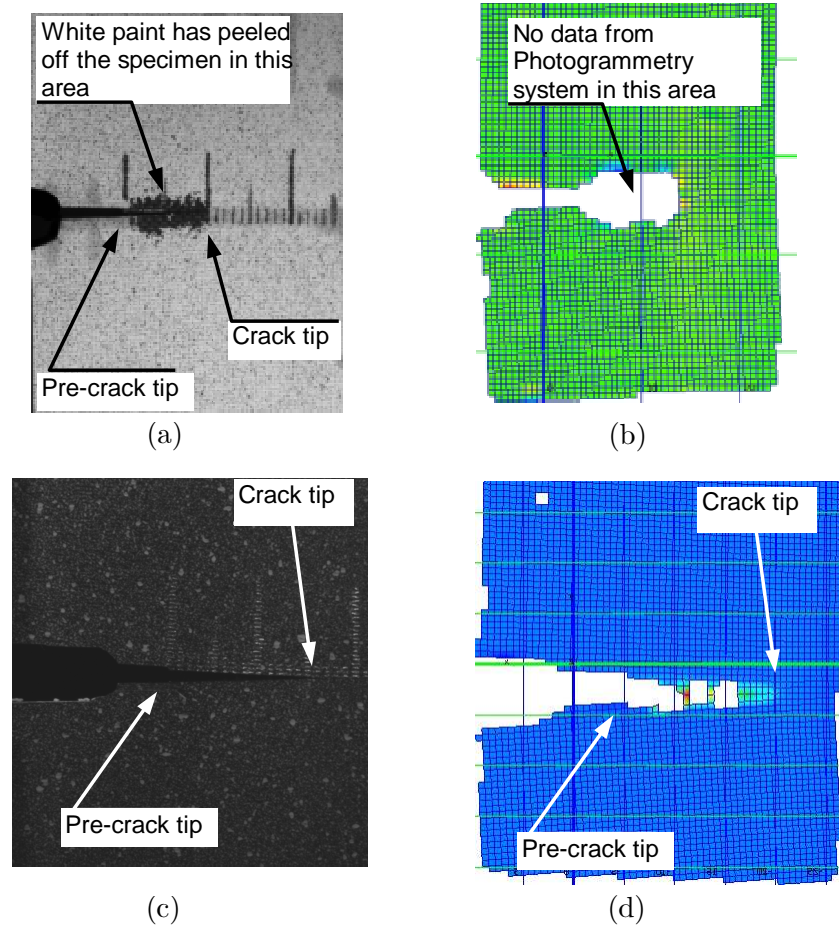


Fig. 6. (a) CT specimen painted white with black speckle pattern; the paint peels off at the crack tip; (b) strain map corresponding to (a) fails to give information close to the crack tip, due to peeling of the paint; (c) CT specimen with white speckle pattern; no peeling is observed at the crack tip; (d) strain map corresponding to (c) allows the identification of the crack tip and does not reveal any other form of damage in the specimen

critical energy release rate obtained for initiation is 91.6 kJ/m^2 with a standard deviation of 6.7%. Since the R-curves seem to converge after $a \approx 34 \text{ mm}$, a propagation value for the critical energy release rate can be defined. The average propagation critical energy release rate is 133 kJ/m^2 with a standard deviation of 15.7%.

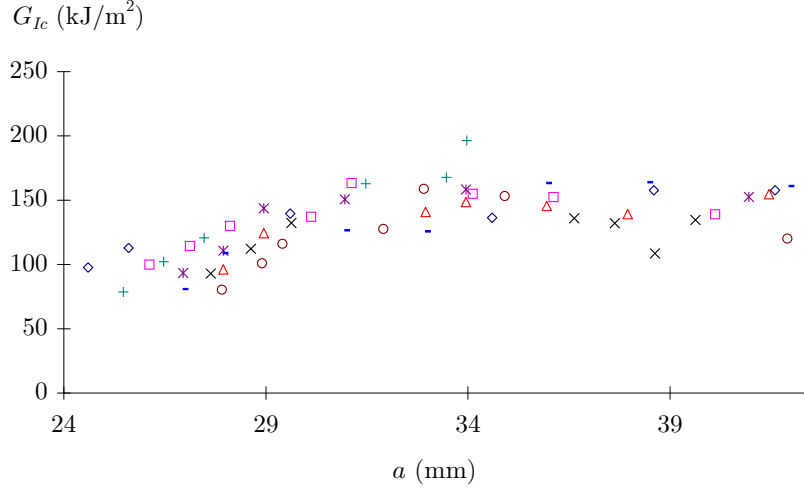


Fig. 7. R-curve for the tensile fracture toughness tests; each symbol-type corresponds to a different specimen

6.2 Compressive tests

For all but one of the CC specimens tested, the kink band grew smoothly during the whole test (approximately 20 mm of kink-band growth). In order to use the area method to determine the critical energy release rate, the unloading curve was recorded after kink-band growth. Since no peeling of the white ink occurred in compression, a black speckle on white background was used for all tests.

The TV monitor, providing a magnified view of the region where the kink band was growing, proved to be ineffective in locating the tip of the damaged area. In fact, the tip of the kink band was barely recognizable on a still image, as shown in Figs. 8(a)-(c) of successive pictures taken by the photogrammetric system. Using the photogrammetric system, the strain gradient proved useful to identify the existence of the kink band, but the identification of the kink-band tip was not trivial, as shown in Fig. 8(d). However, the identification of

the tip of the damaged area was possible using the photogrammetric system in a different way. A picture was taken automatically by the system every 5 s and the event marker was used to identify the load corresponding to that picture. The tip of the damaged area could then be identified by switching repeatedly between two successive images taken by the system. This dynamic viewing process showed the tip of the damaged area very clearly, since the human eye has evolved to easily identify movement and thus the difference between two pictures. As shown in Figs. 8(e) and (f), this difference can also be obtained digitally, by subtracting two consecutive pictures taken by the photogrammetric system.

The R-curves obtained from the compressive tests are shown in Fig. 9. The average critical energy release rate obtained for initiation is 79.9 kJ/m^2 with a standard deviation of 7.7%. Using the area method, the average propagation critical energy release rate is 143 kJ/m^2 with a standard deviation of 10.5%. However, as detailed in the next section, this propagation value is not a reliable measure of critical energy release rate for kink-band propagation.

7 Discussion

7.1 Data reduction

The difference in the critical energy release rate obtained using the data reduction from ASTM standard E399 [10] for metals (isotropic material) and the FE approach is found to be significant (11.0% for the material, layup and geometry considered here), even though E_x and E_y were equal for the laminate layup used in these tests. Therefore, the use of this standard for orthotropic

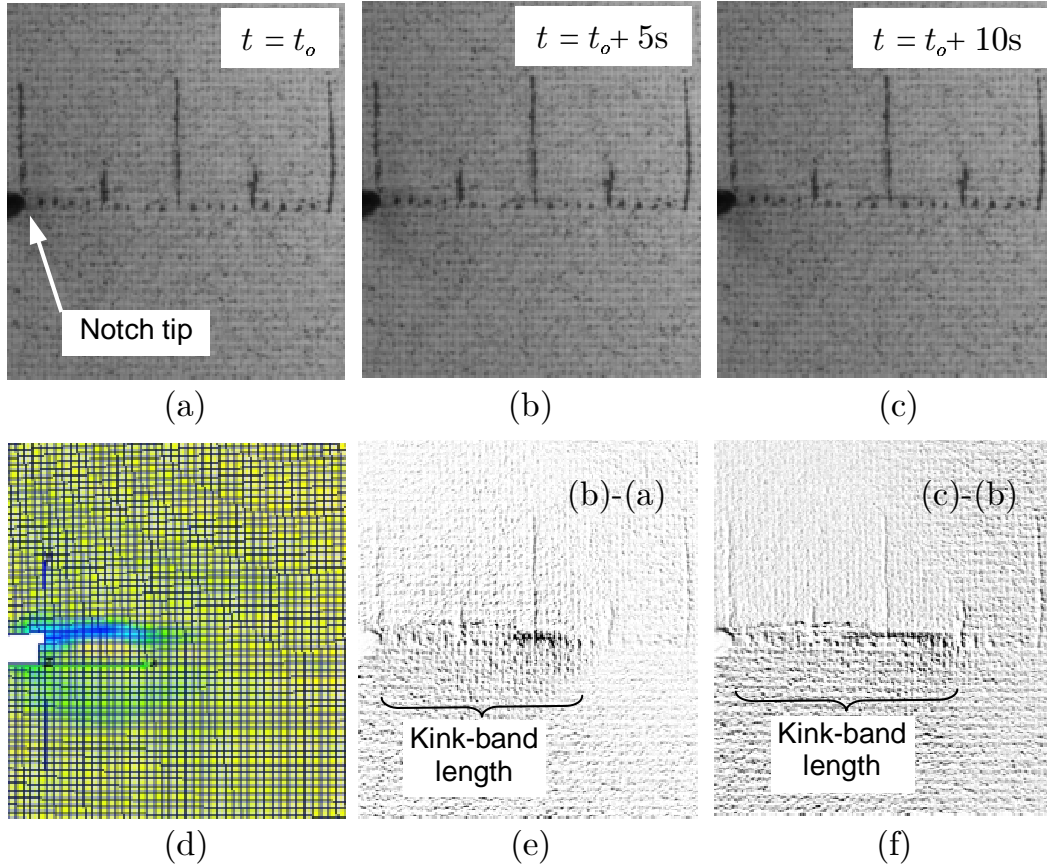


Fig. 8. (a) CC specimen during kink-band propagation at time $t = t_o$, (b) at time $t = t_o + 5$ s, (c) at time $t = t_o + 10$ s; (d) strain map corresponding to (b); (e) difference between pictures (a) and (b); (f) difference between pictures (b) and (c)

composite materials is not recommended.

7.2 Tensile tests

The specimen R-curves shown in Fig. 7 present the same trend even though the pre-crack lengths vary. The G_{Ic} initiation values show good agreement and then the curves all exhibit a positive trend over the next 4 – 8 mm of crack growth. Fig. 10(a) shows a Scanning Electron Microscope (SEM) image of the typical fracture surface. It is not an entirely planar fracture surface,

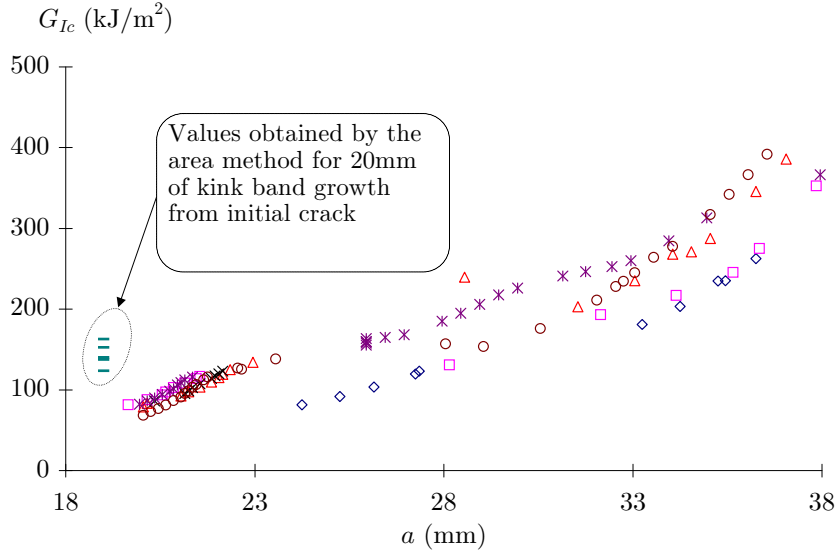


Fig. 9. R-curve for the compressive fracture toughness tests; each symbol-type corresponds to a different specimen

as it exhibits a limited amount of fibre-pullout in the 0° plies. This pullout process could have created a fibre-bridged zone in the wake of the advancing crack tip and the growth and eventual stabilization of this bridged zone could account for the trend observed in the R-curves.

The higher magnification image shown in Fig. 10(b) indicates that the 0° fibres immediately adjacent to the 90° ply interface are fractured without pullout. The 0° fibres further away from the 90° ply interface have undergone pullout with the fibre fracture occurring at some distance from the fracture surface in the 90° ply. The fracture features on the surface in the interface between the 90° and 0° plies shown in Fig. 10(b) indicate that the fracture occurred first in the 90° ply and then propagated into the 0° ply.

Even though there is no visible damage away from the crack plane, as shown by the C-scan in Fig. 11(a), the interaction of the 90° and 0° plies may significantly affect the fracture process during propagation and so the propagation

value of fracture toughness is likely to be layup dependent.

It may well be that the lower initiation value of G_{Ic} is associated with an initial planar fracture from the pre-crack plane without any significant fibre pullout—and if this is the case, then the initiation value would be layup independent. The mechanisms associated with the initiation and propagation fracture processes need further investigation to fully establish their layup dependence.

7.3 Compressive tests

An increasing trend is exhibited by all the compressive-loading R-curves (Fig. 9) and there is a good agreement in the initiation values. The positive trend in the R-curves, Fig. 9, can be explained by the contact forces in the kink-band faces. However, the presence of these contact forces does not explain why the fracture toughnesses obtained by the area method are higher than the initiation values determined using Eqs. 6 and 8. In order to investigate whether the difference is due to other damage modes (delamination, kink-band broadening, crushing), C-scans of the failed specimens were performed, and several micrographs at different locations along the kink-band path were obtained. The C-scan, Fig. 11(b), clearly shows that kink-band propagation has been accompanied by delamination growth.

Several micrographs were taken from the tested specimens at specific cross-sections, as shown in Fig. 12. Those taken from cross-section ‘A,’ i.e. next to the tip of the kink band, are shown in Fig. 13, while those taken in cross-section ‘B,’ i.e. about 10 mm behind the tip of the kink band, are shown in

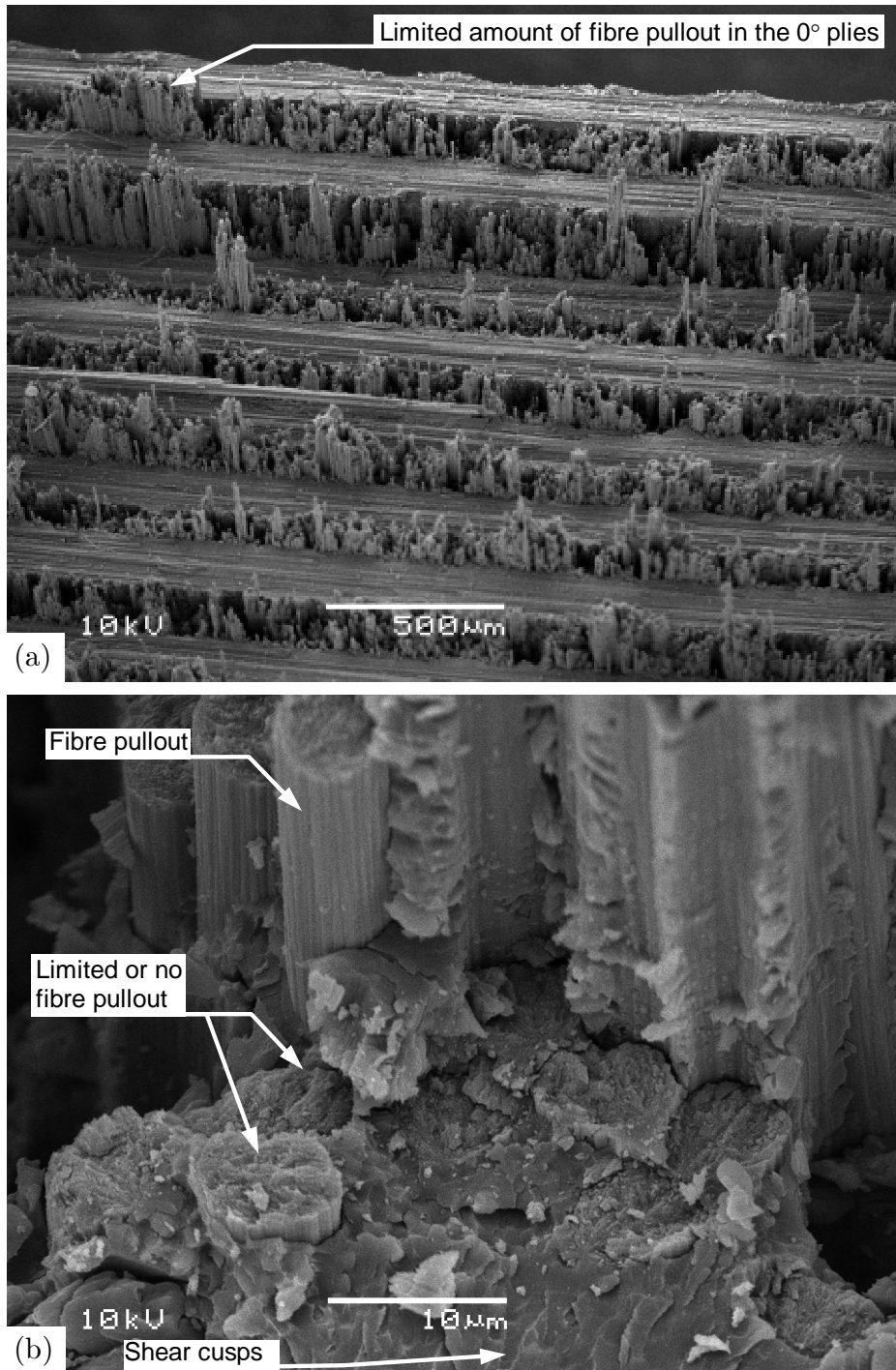


Fig. 10. (a) SEM micrograph of the CT specimen's fracture surface; (b) the magnitude of fibre pull out depends on the distance to the 90° layers

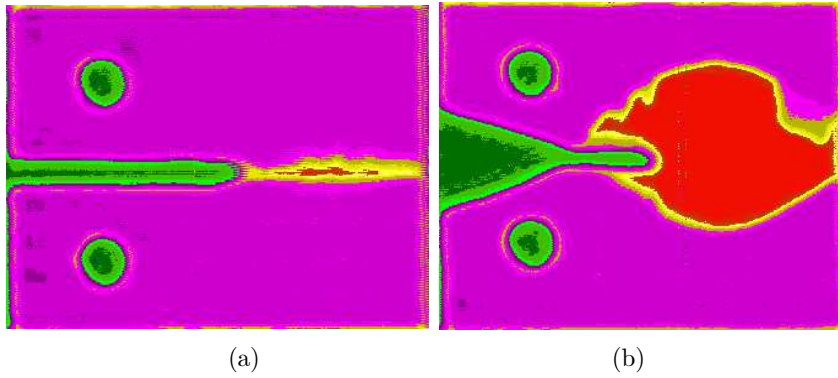


Fig. 11. C-scan of a (a) CT specimen and (b) CC specimen

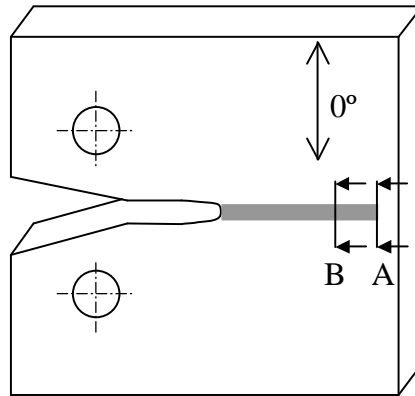


Fig. 12. Cross-sections 'A' and 'B' for the micrographs shown in Figs. 13 ('A') and 14 ('B')

Fig. 14. Fig. 13(a) shows a 0° ply in which the kink band has not yet fully developed. Matrix cracking in the adjacent 90° plies and fracture in some of the 0° fibres can be seen and these will ultimately develop into an out-of-plane kink band similar to those shown in Fig. 13(b) and in magnified detail in Fig. 13(c). Fig. 13(d) shows the matrix cracking and delamination which occurs in the 90° plies between neighboring kink bands.

Turning to Fig. 14, it is clear that the scale of the fibre and matrix damage is now more extensive than that close to the kink-band tip shown in Fig. 13. In Fig. 14(a), the 0° plies clearly bent and in Fig. 14(b) the bending has caused failure in the 0° fibres, i.e. the damage zone is broadening beyond

that associated with the initial kink-band formation. Figs. 14(c) and (d) show delaminations which have been wedge opened by damaged material. These delaminations grow significantly beyond the kink-band region, as detected by the C-scan image shown in Fig. 11(b).

These findings, from analysis of the micrographs and C-scan images, imply that the values of critical energy release rate obtained by the area method do not describe accurately the energy absorbed in kink-band formation, since other significant failure modes have taken place. The initiation values seem to be the best measure of the critical energy release rate associated with kink-band formation.

8 Conclusions

This paper has investigated an experimental procedure to obtain the fracture toughness associated with the fibre-dominated failure modes, using CT and CC tests. It has been shown that the data reduction process based on the stress intensity factor for isotropic materials should not be used, and FE was found to be a valid alternative. Initiation toughness values for both tensile fibre failure and for kink-band formation were obtained. For the tensile mode, propagation toughness values were also measured. For kink-band formation, propagation values cannot be obtained directly from a stress intensity factor approach because the contact stresses in the faces of the kink band cannot be easily accounted for; the area method also failed to produce meaningful results due to kink band broadening and delamination. The toughness measured for both the tensile and compressive modes may well be layup dependent and further investigation is required.

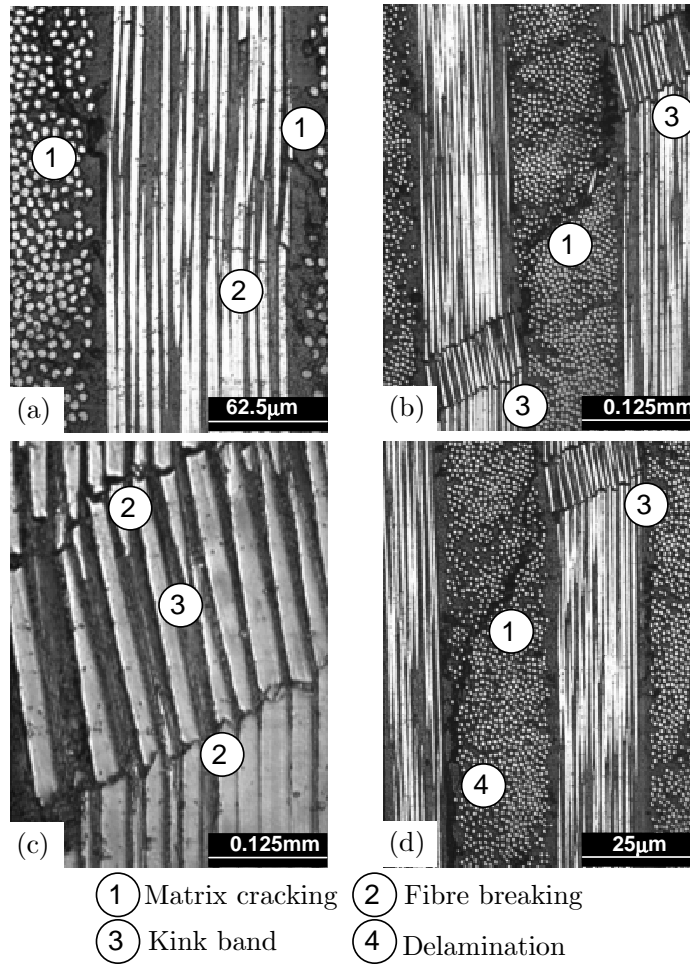


Fig. 13. Micrographs of the kink band in a CC specimen taken at section 'A', see Fig. 12

Acknowledgements

The funding of this research from the Portuguese Foundation for Science and Technology is gratefully acknowledged, as well as the help of Dr. Emile Greenhalgh and Ms. Victoria Bloodworth with the SEM.

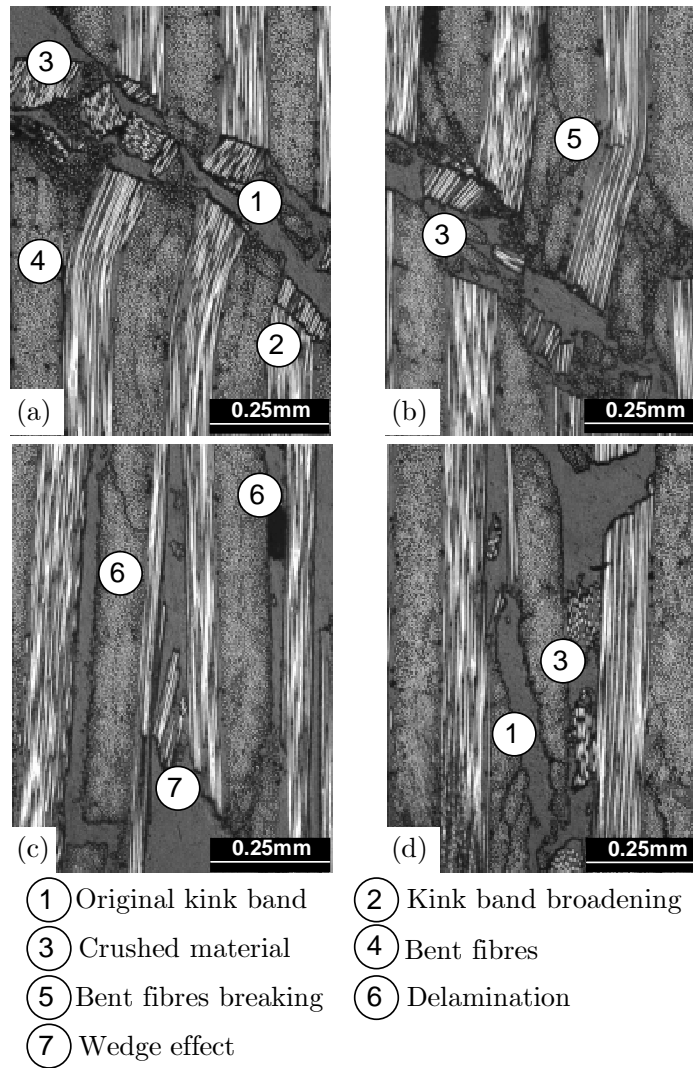


Fig. 14. Micrographs of the kink band in a CC specimen taken at section 'B', see Fig. 12

References

[1] D. R. Leach, J. C. Seferis, Intrinsic characterization of continuous fibre reinforced thermoplastic composites—1: Toughness characterization of carbon fibre/ polyether ether ketone (CF/PEEK) laminates, *Pure and Applied Chemistry* 63 (11) (1991) 1609–1625.

[2] S. Jose, R. K. Kuma, M. K. Jana, G. V. Rao, Intralaminar fracture toughness

of a cross-ply laminate and its constituent sub-laminates, *Composites Science and Technology* 61 (8) (2001) 1115–1122.

- [3] C. Soutis, N. A. Fleck, P. A. Smith, Failure prediction technique for compression loaded carbon fibre-epoxy laminate with an open hole, *Journal of Composite Materials* 25 (1991) 1476–1498.
- [4] C. Soutis, P. T. Curtis, N. A. Fleck, Compressive failure of notched carbon fibre composites, *Proceedings of the Royal Society London A* 440 (1993) 241–256.
- [5] C. Soutis, P. T. Curtis, A method for predicting the fracture toughness of CFRP laminates failing by fibre microbuckling, *Composites Part A* 31 (2000) 733–740.
- [6] J. Ratcliffe, W. Jackson, J. Schaff, Compression strength prediction of impact-damaged composite sandwich panels, in: *American Helicopter Society 60th Annual Forum*, Baltimore, MD, 2004.
- [7] W. C. Jackson, J. G. Ratcliffe, Measurement of fracture energy for kink-band growth in sandwich specimens (paper no. 24), in: *Composites Testing and Model Identification, CompTest2004*, University of Bristol, Bristol, UK, 2004.
- [8] K. D. Cowley, P. W. R. Beaumont, The interlaminar and intralaminar fracture toughness of carbon-fibre/polymer composites: The effect of temperature, *Composite Science and Technology* 57 (1997) 1433–1444.
- [9] A. C. Garg, Intralaminar and interlaminar fracture in graphite/epoxy laminate, *Engineering fracture mechanics* 23 (4) (1986) 719–733.
- [10] Standard Test Method for Plane-Strain Fracture Toughness of Metallic Materials, ASTM E399-90, *Annual Book of ASTM Standards* 03.01 (1993) 407–528.
- [11] P. C. Paris, G. C. Sih, Stress analysis of cracks, fracture toughness and applications, STP-381, ASTM (1969) 30–83.

- [12] Abaqus, Inc., 1080 Main Street, Pawtucket, R. I. 02860, Abaqus 6.4-1 (2003).
- [13] S. T. Pinho, P. Robinson, L. Iannucci, Developing a four point bend specimen to measure the mode I intralaminar fracture toughness of unidirectional laminated composites, Submitted to Composites Science and Technology.